Engineering and Technology Journal e-ISSN: 2456-3358

Volume 10 Issue 12 December-2025, Page No.-8269-8280

DOI: 10.47191/etj/v10i12.27, I.F. – 8.482

Optimised Silver-Doped Banana Peel Biosorbent for Marble Effluent: Adsorption Properties and Response Surface Methodology

O.A. Olabemiwo.[1], O.S. Olaniyan.[2], S. A. Adebayo.[3], A. A. Azeez.[4], L. O. Babalola.[5], O. R. Lawal[6], A. O. Adebayo.[7]

[1,2,3]Department of Civil Engineering, Ladoke Akintola University of Science and Technology, Ogbomoso, Nigeria.

[4,5,6,7]Department of Civil Engineering, Federal University of Technology, Akure, Nigeria.

ABSTRACT: Banana peels, a widely available agro-waste, are rich in lignocellulosic matrices and oxygenated functional groups that enable effective adsorption of metal ions and dyes. Marble industry effluents, containing high suspended solids, turbidity, and dissolved metals, present environmental hazards. This study aimed to synthesise silver-doped banana peel (AgNP-BP) composites and optimise their application for heavy metal removal from marble wastewater. Dried banana peels were pulverised, extracted, and used to synthesise AgNPs via green reduction with 1 mM $AgNO_3$. The biosorbent was doped with AgNPs, oven-dried, and applied in a laboratory-scale sand filtration system. Effluent filtration was conducted under varying contact times (15–120 min), pH (6.5–9.5), and initial concentrations (25–100 mg/L). Physicochemical parameters and heavy metals (Zn, Mn, Cd, Pb, Ca, Fe) were analysed. Removal efficiency (RE) and adsorption capacity (q_e) were calculated, and Response Surface Methodology (RSM) optimised process variables. Results showed TDS ranged 198–278 mg/L, EC 430–590 µS/cm, DO 11–11.6 mg/L, BOD 8–15.8 mg/L, and COD 150–245 mg/L after treatment. Zn and Pd were reduced to 1.0–1.95 mg/L and 0.03–0.05 mg/L, while Mn and Cd slightly increased to 0.05–0.125 mg/L and 0.012–0.14 mg/L. Optimal removal occurred at pH 7.5–8.5, contact time 60–120 min, and initial concentrations 25–75 mg/L. Regression models accurately predicted responses, and response surface plots confirmed the significance of linear, quadratic, and interaction terms. In conclusion, AgNP-BP composites effectively reduced Zn and Pd in marble effluents and can be recommended for sustainable, low-cost wastewater treatment, particularly under controlled pH, contact time, and concentration conditions.

KEYWORDS: Banana peel, Silver nanoparticles, Marble effluent, Heavy metals, Adsorption, Response Surface Methodology.

1. INTRODUCTION

Banana peels, an abundant agricultural residue, have attracted considerable attention as low-cost biosorbents due to their porous lignocellulosic matrix and the presence of oxygenated functional groups (e.g., hydroxyl, carboxyl, and carbonyl) that facilitate binding of ionic and organic contaminants; empirical studies have demonstrated effective removal of dyes and metal ions using raw, chemically activated, or thermally modified banana peel materials (Asemave et al., 2023; Boyle et al., 2025). Furthermore, the surface chemistry and textural properties of banana peel derivatives can be tailored by physical or chemical activation to increase surface area and expose additional binding sites, thereby improving uptake capacity and selectivity for targeted pollutants (Gupta et al., 2025). In addition, contemporary reviews of biosorbent preparation emphasize that valorisation of agro-waste into functional adsorbents aligns with circular economy goals and yields materials that are both affordable and scalable for decentralized wastewater treatment, which is particularly relevant for industrial effluents in resource-limited settings (Sathasivam et al., 2023; Ejairu et al., 2024).

Chemical modification by incorporation of metallic nanoparticles—notably silver nanoparticles (AgNPs)—has emerged as an effective strategy to enhance the adsorptive and catalytic behaviour of low-cost biosorbents; green synthesis approaches using banana peel extracts both reduce environmental impact and exploit intrinsic phytochemicals as reductants and stabilizers for AgNP formation (Syafiuddin et al., 2020; Sati et al., 2025). Moreover, recent experimental reports indicate that nanoparticle impregnation can alter sorbent kinetics and equilibrium capacities in ways that are favourable for rapid treatment of concentrated industrial discharges, although the extent of enhancement depends on synthesis route, nanoparticle size/distribution, and the nature of target pollutants (Mansour et al., 2022; Ali et al., 2025).

Marble industry effluents constitute a complex waste stream characterised by high suspended solids, elevated turbidity, alkaline pH, calcium-rich slurries, and frequently measurable concentrations of heavy metals and process chemicals, all of which pose risks to aquatic ecosystems, soil quality, and groundwater resources if discharged untreated (Asimullah et al., 2025; Neelab et al., 2022). Consequently, conventional treatment techniques—such as coagulation, sedimentation,

and advanced oxidation—are often used but may be costly, generate secondary wastes (e.g., sludge), or lack adaptability for small and medium enterprises that dominate marble processing in many regions (Sathya et al., 2022). In this context, adsorptive remediation using tailored biosorbents could deliver a cost-effective complement or alternative, by targeting dissolved metals and colloidal particulates while enabling material valorisation and potential on-site deployment (Kunwar, 2022; Thakur and Kumar, 2024).

Despite demonstrated potential, there remains a clear problem: existing studies on banana-based biosorbents and nanoparticle-enhanced composites seldom target marble effluents specifically, and those that do rarely combine green AgNP doping with systematic RSM optimisation and comprehensive kinetic modelling to produce an operationally treatment recipe for slurry-dominated wastewater. Consequently, data gaps persist regarding the optimum synthesis parameters (e.g., Ag loading, impregnation method, post-treatment activation), the interplay between sorbent structural features and adsorption kinetics for calcium- and particulate-rich matrices, and the sorbent reusability and fouling behavior under conditions representative of marble processing effluents. Thus, a focused investigation is required to generate experimentally validated models that link synthesis and process variables to performance metrics relevant for marble wastewater management, including removal of colloidal solids, dissolved metal fractions, and operational stability over repeated cycles.

Addressing this is significant because an optimized, silver-doped banana peel bio sorbent—developed via green synthesis and parameterized through RSM and adsorption kinetics—could provide a low-cost, locally sourced treatment option that reduces pollutant discharge from marble workshops, diminishes reliance on chemical coagulants, and valorizes agricultural waste while maintaining high removal efficiencies; such outcomes align with sustainable water management objectives and circular-economy imperatives in industrial regions (Brears, 2025; Obiuto, et al., 2024). Consequently, this research has the potential to influence both academic understanding of Nano-enhanced biosorption mechanisms and practical decisions in industrial wastewater governance.

2. METHODOLOGY

2.1 Sample Collection and Preservation

This research was conducted using materials sourced from Ogbomoso and Igbeti in Oyo State, Nigeria. Unripe banana peels were obtained from a small-scale plantain-chips processing facility located in the Randa Area of Ogbomoso. Industrial marble effluent was collected from an active marble mining and processing site at Igbeti. Fresh unripe banana peels were collected in sterile polyethylene bags and immediately transported to the laboratory to prevent microbial degradation. Effluent samples were collected using pre-sterilized, high-density polyethylene kegs with a 15 L capacity. Each container was thoroughly rinsed with the effluent before final collection.

Immediately after sampling, the kegs were sealed, labelled, stored in an insulated cooler containing ice packs, and transferred to FEMTOP Laboratory, Ologuneru Road, Ibadan, for preservation at 4 °C in a laboratory refrigerator pending analysis. The freshly obtained banana peels were washed thoroughly with potable water and subsequently with distilled water to remove surface debris. The peels were sliced into smaller pieces to increase surface area and air–sun dried outdoors for four days until the moisture content reduced sufficiently, indicated by a visible colour change from green to brownish-black as shown in Plate 1 and 2 respectively. The dried material was pulverized into a fine powder using a Grinding Mill and stored in airtight polypropylene containers as shown in Plate 3.

A measured mass of 1.0 g of the powdered biomass was added to 500 mL of distilled water and heated at 60 °C for 1 hour using a Water Bath. The mixture was filtered using filter paper to obtain the aqueous extract. Silver nanoparticles were synthesized by adding 500 mL of this extract to 1000 mL of 1 mM analytical-grade silver nitrate ($AgNO_3$) solution as depicted in Plate 4. The reaction was carried out in a borosilicate glass reaction vessel under ambient conditions.

2.2 Doping of Banana Peel Biosorbent with Silver Nanoparticles

A total of 100 g of the powdered banana peel was mixed with 1000 mL of the freshly synthesized AgNP solution in a 2 L Erlenmeyer flask. The mixture was mechanically agitated overnight using a Magnetic Stirrer. The AgNP-loaded biomass was recovered through filtration and dried at 110 °C for 10 hours in a Universal Oven. The dried composite material, representing the silver-doped banana peel biosorbent, was stored in airtight containers before application.

Plate 1: Freshly Collected Unripe Banana Peels

Plate 2: Sun-Dried Unripe Banana Peels

Plate 3: Pulverized Unripe Banana Peel Powder

Plate 4: Aqueous Extract of Unripe Banana Peel

2.3 Application of Marble Effluent to the Filtration Bed

A laboratory-scale sand filter bed was constructed using a rectangular borosilicate glass tank arranged in two vertical cells . The upper compartment consisted of five graded layers: sharp sand, ground banana peel powder, ¾-inch granite, ½-inch granite, and 1-inch granite. The lower cell, equipped with a valve-tap outlet, served as the collection unit. One litre of marble effluent was introduced into the upper cell and allowed to percolate as depicted in Plate 5. Retention times were recorded using a digital stopwatch. Filtrates from the first, second, and third passes were collected and later subjected to physico-chemical analysis.

2.4 Characterization of the Silver Nanoparticles (AgNPs)

The synthesized silver nanoparticles (AgNPs) were characterized using Fourier Transform Infrared Spectroscopy (FTIR) to identify the functional groups responsible for stabilizing the nanoparticles. The analysis was conducted with an FTIR Spectrometer operated within the range of 4000–400 cm^{-1}.

Plate 5: Laboratory-Scale Sand Filtration Unit

Before scanning, the dried AgNP sample was homogenized with spectroscopic-grade potassium bromide (KBr) and compressed into a transparent pellet to ensure optimal signal transmission. The pellet was then placed in the sample compartment, and the spectrum was recorded at a resolution of 4 cm^{-1}. The resulting absorption bands were examined to determine the presence of biomolecules, such as hydroxyl, carbonyl, or amine groups, which contributed to the reduction and capping of silver ions during biosynthesis. Furthermore, the spectra were compared with reference functional group libraries to confirm structural interactions between the banana peel extract and the AgNPs.

2.5 Characterization of Heavy Metal

Effluent samples were digested prior to analysis using the U.S. EPA nitric acid digestion method. A 50 mL portion of the sample was placed in a 250 mL borosilicate conical flask, followed by addition of 10 mL concentrated HNO_3. The mixture was gently boiled on a Thermo Cimarec with Hot Plate and progressively evaporated. Additional nitric acid was introduced until the solution turned clear. After cooling, 5 mL of HCl was added, and the digest was diluted to 50 mL with distilled water. Heavy metal concentrations (Mn, Cd, Pb, Fe, Ca, and Zn) were quantified using a Flame Atomic Absorption Spectrophotometer.

2.6 Removal efficiency and Adsorption capacity

All adsorption experiments were performed in triplicate. Removal efficiency (RE) was computed using:

$$\text{RE}\ (\%) = \frac{C_O - C_t}{C_O} \text{ x } 100$$

Where; C_O = initial concentration (mg/L) and C_t = concentration at time t.

Adsorption capacity (q_e) was computed using:

$$q_e = \frac{(C_O - C_e)V}{m} \text{ x } 100$$

where C_e = equilibrium concentration (mg/L), V = solution volume (L), and m = mass of biosorbent (g).

2.7 Statistical Modelling

Optimization of experimental parameters (contact time, pH, and initial metal concentration) was carried out using Response Surface Methodology (RSM) implemented through Design-Expert Software Version 13.

3. RESULT AND DISCUSSIONS

3.1 Characteristics of the Silver Nanoparticles (AgNPs)

Fourier Transform Infrared Spectroscopy (FTIR) provided insight into the functional groups that stabilized the biosynthesized AgNPs. As illustrated in Figure 1, the spectrum showed absorption peaks at 3439.09, 2922.17, 2854.27, 2360.02, 2342.04, 1734.15, 1636.06, 1457.32, and 1057.63 cm^{-1}, reflecting biomolecules present in the banana peel extract. The broad band at 3439.09 cm^{-1} corresponded to O–H or N–H stretching, indicating the involvement of hydroxyl or amine groups in nanoparticle stabilization (Ajayi et al., 2020). The C–H stretching vibrations at 2922.17 and 2854.27 cm^{-1} aligned with typical alkane structures, while the peaks at 2360.02 and 2342.04 cm^{-1} suggested carbonyl-related stretching (Singh & Mehta, 2018). The 1636.06 cm^{-1} band signified N–H bending, whereas the 1457.32 and 1057.63 cm^{-1} peaks indicated alkane bending and C–O stretching, respectively. These observations confirmed that organic functional groups acted as reducing and capping agents during nanoparticle formation (Oluwaseun et al., 2021).

Dynamic light scattering (DLS) further revealed an average particle size of 141.4 nm with a polydispersity index of 0.361, reflecting a moderate size distribution and acceptable nanoparticle stability. Comparable particle sizes have been reported in other green synthesis studies, supporting the reliability of the present results and reinforcing the role of biologically derived compounds in influencing nanoparticle morphology and uniformity.

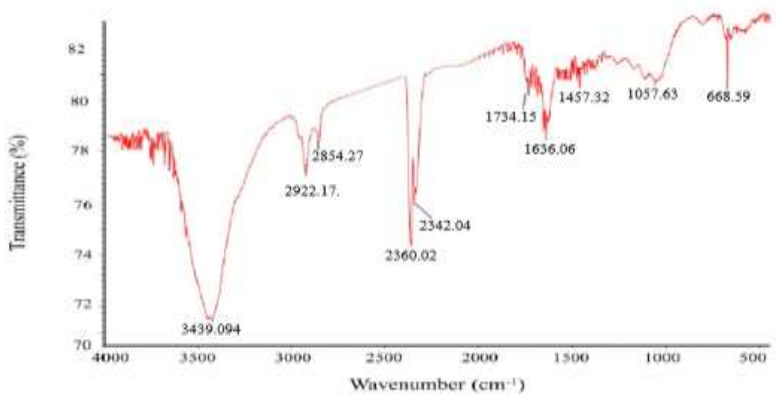

Figure 1: Fourier Transform Infrared Spectroscopy (FTIR) Spectra of Synthesized Silver Nanoparticles.

3.2 Characterization of Heavy Metal

The initial physicochemical characteristics of the marble effluent showed that the raw wastewater was highly alkaline, with pH values ranging from 8.52 to 8.54, whereas treatment reduced it to a near-neutral range of 7.81 to 7.83, indicating improved suitability for discharge. This reduction aligns with findings by Khan et al. (2023), who reported similar pH moderation in marble-processing effluents following adsorption treatment. Dissolved oxygen declined from 12.0–13.0 mg/L to 9.0–10.5 mg/L, corresponding to a 25% reduction and an adsorption capacity of 3.0–3.5 mg/g. Although the decline suggests increased oxygen demand after treatment, the DO values remained within acceptable limits for surface water quality. Additionally, colour changed from colourless to light brown and odour intensified slightly, indicating that partial oxidation or suspended fines may have developed during treatment.

The concentration of dissolved and ionic species exhibited a notable increase after treatment. TDS rose sharply from 320–324 mg/L to 835–841 mg/L, while electrical conductivity increased from 651–656 µS/cm to 1680–1701 µS/cm, giving negative removal efficiencies of –160.94% and –158.06%, respectively, and high negative adsorption capacities as shown in Table 1. Turbidity (asm) similarly increased from 0.103–1.135 to 0.254–0.284, also giving a negative removal efficiency. These increases suggest desorption of fines or release of soluble ions from the adsorbent, contrasting with the reductions reported by Hou et al. (2020), who achieved substantial decline in TDS and EC using natural adsorbents. Turbidity measured in NTU remained above 100 both before and after treatment, although a slight percentage decrease was recorded, showing limited improvement in particulate removal. The pronounced rise in total solids from 6.5 mg/L to 9.5–700 mg/L and total suspended solids from 210 mg/L to 68–200 mg/L further confirms the possibility of particle detachment from the treatment medium, contradicting expectations for conventional adsorption systems.

The organic load, measured by BOD and COD, increased considerably after treatment. BOD rose from 20.5–25.4 mg/L to 60.50–64.21 mg/L, while COD increased from 270–285 mg/L to 350–365 mg/L, showing negative removal efficiencies and negative adsorption capacities. This behaviour may indicate the introduction of biodegradable organic residues from the treatment material, similar to observations by Ambaye et al. (2021), who reported organic leaching from some biosorbents. In contrast, some metals such as Zn and Pd showed substantial reductions: Zn decreased from 4.29–5.02 mg/L to 1.80–1.89 mg/L (58.04% removal), while Pd declined from 0.08–0.12 mg/L to 0.03–0.05 mg/L (62.5% removal), with positive adsorption capacities. Conversely, Mn and Cd concentrations increased significantly after treatment, with Mn rising from 0.180–0.184 mg/L to 0.647–0.651 mg/L and Cd increasing from 0.002–0.003 mg/L to 0.012–0.14 mg/L, which may indicate metal release from the adsorbent matrix and is inconsistent with typical adsorption behaviour.

The carbonate-related parameters demonstrated marginally improved outcomes. Alkalinity reduced from 195–205 mg/L to 165–170 mg/L, corresponding to a 15.38% removal and adsorption capacity of 25–40 mg/g, reflecting partial neutralisation. Hardness similarly decreased from 110–115 mg/L to 95–100 mg/L, giving a 13.64% removal, while calcium concentration exhibited only a slight increase from 2.761–3.125 mg/L to 2.767–2.883 mg/L, representing minimal change. These results show moderate performance in reducing scale-forming ions, aligning partially with the trends reported by Lin et al., (2020), who achieved modest reductions in hardness using locally sourced adsorbents. Settleable solids also decreased from 10.8–200 mg/L to 4.8–140 mg/L, giving 55.5% removal and positive adsorption capacities, indicating effective sedimentation of larger particulates despite the large fluctuations in total solids. Collectively, the mixed performance across parameters suggests that while the treatment system demonstrated selective metal removal, it may require optimisation to reduce dissolved solids, organic load, and residual particulates.

Table 1: Characteristics of Marble Effluent before and after Treatment

Parameters	Before Treatment	After Treatment	Removal Efficiency (RE, %)	Adsorption Capacity (q_e, mg/g)
pH	8.52–8.54	7.81–7.83	8.33 (decrease)	–
TDS (mg/L)	320–324	835–841	–160.94 (increase)	–515–521
EC (µS/cm)	651–656	1680–1701	–158.06 (increase)	–1029–1055
Turbidity (asm)	0.103–1.135	0.254–0.284	–146.6 (increase)	–
Turbidity (NTU)	>100	>100	8.33 (decrease)	–
Colour	Colourless	Light brown	–	–
Odour	Offensive	Highly offensive	–	–
DO (mg/L)	12.0–13.0	9.0–10.5	25	3.0–3.5
BOD (mg/L)	20.5–25.4	60.50–64.21	–195.12 (increase)	–40 to –38
COD (mg/L)	270–285	350–365	–29.63 (increase)	–80 to –75
Zn (mg/L)	4.29–5.02	1.80–1.89	58.04	2.40–3.22

Mn (mg/L)	0.180–0.184	0.647–0.651	–259.44 (increase)	–0.47 to –0.50
Cd (mg/L)	0.002–0.003	0.012–0.14	–500 (increase)	–0.01 to –0.14
Pd (mg/L)	0.08–0.12	0.03–0.05	62.5	0.03–0.09
Alkalinity (mg/L)	195–205	165–170	15.38	25–40
Hardness (mg/L)	110–115	95–100	13.64	10–15
Ca (mg/L)	2.761–3.125	2.767–2.883	–0.22 (increase)	–0.01 to –0.12
TTS (mg/L)	35.0–45.0	570–590	–1528.57 (increase)	–535–525
Total Solids (mg/L)	6.5	9.5–700	–46.15 (increase)	–3000 to –693,500
Suspended Solids (mg/L)	210	68–200	96.76	209,320–10,000
Settleable Solids (mg/L)	10.8–200	4.8–140	55.5	6,000–60,000

3.3 Process Optimization

The post-treatment water quality results across the three operational variables demonstrate clear trends that reflect the influence of initial concentration, solution pH, and contact time on contaminant removal. As the initial concentration increased from 25 to 100 mg·L⁻¹, TDS declined from 256 to 198.5 mg·L⁻¹, while EC similarly reduced from 524 to 430 µS·cm⁻¹, indicating improved ionic removal at higher loading. Dissolved oxygen also reduced slightly from 11.6 to 11 mg·L⁻¹, yet remained within acceptable limits as illustratedin Table 2. Organic parameters behaved differently, as BOD increased from 8.4 to 14 mg·L⁻¹ and COD rose from 160 to 235 mg·L⁻¹, implying gradual sorbent saturation at elevated concentrations. The metals Zn and Mn showed an upward drift from 1.15 to 1.95 mg·L⁻¹ and 0.055 to 0.125 mg·L⁻¹, respectively, supporting the possibility of site saturation at high contaminant loads. This trend contrasts with findings by van Linden et al., (2020), who noted enhanced metal removal at higher initial concentrations due to stronger concentration gradients driving diffusion. Furthermore, alkalinity, hardness, calcium, and total solids showed steady increases, indicating that matrix dissolution may have contributed to residual mineral enrichment in the treated water.

The influence of pH revealed an optimal treatment window around neutral to slightly alkaline conditions. At pH 7.5 and 8.5, TDS dropped to 242 and 228.5 mg·L⁻¹, respectively, compared with 270 mg·L⁻¹ at pH 6.5 and 245 mg·L⁻¹ at pH 9.5 as illustrated in Table 3. EC followed a similar trend, reaching its lowest value of 475 µS·cm⁻¹ at pH 8.5. DO increased to 11.8 mg·L⁻¹ at pH 8.5, reflecting improved oxygen retention under favourable ionic conditions. BOD and COD decreased substantially at pH 7.5 and 8.5, falling to 9 and 8.2 mg·L⁻¹ for BOD, and 165 and 150 mg·L⁻¹ for COD, indicating improved removal of biodegradable and oxidisable organics. Metal concentrations also reached minimal values at pH 8.5, with Zn at 1.02 mg·L⁻¹ and Mn at 0.05 mg·L⁻¹, consistent with optimal adsorption of divalent ions under moderately alkaline conditions. Additionally, alkalinity, hardness, calcium, and total solids were lowest at pH 8.5, confirming that extreme acidity or alkalinity suppressed treatment efficiency.

The effect of contact time showed a progressive improvement in water quality as exposure increased from 15 to 120 minutes. TDS declined from 278 to 232 mg·L⁻¹, while EC reduced from 590 to 505 µS·cm⁻¹, indicating sustained mass transfer with extended interaction. DO increased from 11 to 11.6 mg·L⁻¹, suggesting reduced microbial or oxidative demand as contaminants were progressively removed. BOD and COD both decreased sharply, falling from 15.8 to 9.2 mg·L⁻¹ and from 245 to 165 mg·L⁻¹, respectively, reflecting the time-dependent nature of organic adsorption. Metals followed the same declining pattern, with Zn dropping from 1.9 to 1.05 mg·L⁻¹ and Mn from 0.14 to 0.055 mg·L⁻¹ as shown in Table 4. These improvements correspond with the increased availability of active sites over prolonged contact, consistent with the findings of Ismail et al. (2022), who demonstrated that equilibrium metal uptake is typically achieved at longer contact durations. Alkalinity, hardness, calcium, and total solids all decreased steadily as contact time increased, reinforcing that extended adsorption facilitated improved physicochemical stability in the treated effluent.

Table 2: Post-Treatment Water Quality Parameters across Varying Initial Concentrations (mg·L⁻¹)

Parameter (unit)	25 mg·L⁻¹	50 mg·L⁻¹	75 mg·L⁻¹	100 mg·L⁻¹
TDS (mg·L⁻¹)	256	229.4	221	198.5
EC (µS·cm⁻¹)	524	492.5	455	430
DO (mg·L⁻¹)	11.6	11.4	11.2	11
BOD (mg·L⁻¹)	8.4	10.2	12.3	14
COD (mg·L⁻¹)	160	185	210	235
Zn (mg·L⁻¹)	1.15	1.48	1.72	1.95

Mn (mg·L⁻¹)	0.055	0.08	0.1	0.125
Alkalinity (mg·L⁻¹ as $CaCO_3$)	120	135	150	162
Hardness (mg·L⁻¹ as $CaCO_3$)	62	75	86	95
Ca (mg·L⁻¹)	1.45	1.7	1.98	2.2
Total Solids (g·L⁻¹)	5.2	4.8	4.3	4

Table 3: Post-Treatment Water Quality Parameters at Different pH Conditions

Parameter (unit)	**6.5**	**7.5**	**8.5**	**9.5**
TDS (mg·L⁻¹)	270	242	228.5	245
EC (µS·cm⁻¹)	560	505	475	515
DO (mg·L⁻¹)	11.2	11.6	11.8	11
BOD (mg·L⁻¹)	13.5	9	8.2	12
COD (mg·L⁻¹)	220	165	150	205
Zn (mg·L⁻¹)	1.85	1.1	1.02	1.6
Mn (mg·L⁻¹)	0.12	0.06	0.05	0.1
Alkalinity (mg·L⁻¹ as $CaCO_3$)	158	132	118	145
Hardness (mg·L⁻¹ as $CaCO_3$)	92	68	60	80
Ca (mg·L⁻¹)	2.05	1.6	1.42	1.85
Total Solids (g·L⁻¹)	5.8	4.5	4	5

Table 4: Post-Treatment Water Quality Parameters at Varying Contact Times.

Parameter (unit)	**15 min**	**30 min**	**60 min**	**120 min**
TDS (mg·L⁻¹)	278	249	236	232
EC (µS·cm⁻¹)	590	540	515	505
DO (mg·L⁻¹)	11	11.3	11.5	11.6
BOD (mg·L⁻¹)	15.8	12.4	10	9.2
COD (mg·L⁻¹)	245	205	178	165
Zn (mg·L⁻¹)	1.9	1.45	1.2	1.05
Mn (mg·L⁻¹)	0.14	0.09	0.065	0.055
Alkalinity (mg·L⁻¹)	170	145	132	125
Hardness (mg·L⁻¹)	100	82	72	68
Ca (mg·L⁻¹)	2.45	1.95	1.72	1.6
Total Solids (g·L⁻¹)	5.9	4.6	4.1	3.9

3.4 Data Analysis and Statistical Modelling

3.4.1 Data Analysis

The model significance outcomes provide a clear indication of how each response variable reacted to the combined effects of pH, initial concentration, and contact time as shown in Table 5. For TDS and EC, the models produced high sum of squares (1545.87 and 4699.76) and strong F-values (10.72 and 9.09), with corresponding p-values of 0.0008 and 0.0015, confirming strong significance. Time, pH, and concentration were consistently influential as linear terms, while pH^2 emerged as a dominant quadratic factor for both parameters. This behaviour corresponds with the findings of Covington et al. (2023), who reported that ionic and dissolved species often respond non-linearly to pH shifts, particularly near buffering points. Additionally, DO exhibited a significant model ($p = 0.0113$), driven by the linear effects of time and concentration, and influenced by pH^2, reinforcing the central role of aeration dynamics during adsorption.

The behaviour of BOD and COD showed contrasting patterns of significance. The BOD model was not statistically significant ($p = 0.1875$), although pH^2 appeared as a relevant quadratic contributor, indicating a weak but observable curvature effect. COD, however, produced a significant result ($p = 0.0198$), with concentration exerting the strongest linear influence, while both pH^2 and concentration² shaped the quadratic behaviour. This aligns with the observation by Ruan et al., (2023), that organic parameters commonly display concentration-dependent removal pathways due to the sorbent's progressive site saturation. Furthermore, metal responses such as Zn and Mn demonstrated significant

models with p-values of 0.0184 and 0.0161. Time significantly influenced their linear behaviour, while the three quadratic components (A^2, B^2, and C^2) indicated a strong curvature effect across all operating variables, consistent with adsorption systems where metal uptake is highly sensitive to pH and concentration variation.

The remaining parameters—alkalinity, hardness, and calcium—produced models that were not significant (p = 0.1256, 0.0750, and 0.0957, respectively). Even so, all three exhibited a consistent interaction between pH and concentration (AC), demonstrating that although their individual effects were weak, their combined influence contributed meaningfully to system variability. This interaction-driven behaviour has also been highlighted by Esmaeeli et al., (2023), who found that mineral parameters in treated water often respond more to synergistic operational effects than to isolated factor changes. Total solids (TS) stood out with a significant model (p = 0.0028), influenced linearly by time, and quadratically by A^2 and B^2, alongside interactions AB and AC. This indicates a complex structure of dependence where time, pH, and concentration collectively shape solids removal efficiency, reflecting a multilayered response pattern typical of heterogeneous effluent matrices.

Table 5: Summary of Model Significance, Linear and Quadratic Effects, and Interaction Terms for All Response Variables.

Response	Model SS	Model F-value	Model p-value	Significant Linear Factors	Significant Quadratic Factors	Significant Interactions
TDS	1545.87	10.72	0.0008	Time, pH, Concentration	pH^2	–
EC	4699.76	9.09	0.0015	Time, pH, Concentration	pH^2	–
DO	0.2744	5.16	0.0113	Time, Concentration	pH^2	–
BOD	1.95	1.85	0.1875 (NS)	–	pH^2	–
COD	924.96	4.34	0.0198	Concentration	pH^2, Concentration^2	–
Zn	0.9493	4.44	0.0184	Time	A^2, B^2, C^2	–
Mn	0.0090	4.63	0.0161	Time	A^2, B^2, C^2	–
Alkalinity	840.83	2.12	0.1256 (NS)	–	–	AC
Hardness	504.52	2.60	0.0750 (borderline NS)	–	–	AC
Calcium (Ca)	0.2582	2.37	0.0957 (NS)	–	–	AC
Total Solids (TS)	1.62	7.66	0.0028	Time	A^2, B^2	AB, AC

NS = not significant

3.4.2 Regression Model Equations for Each Response

The regression model equations illustrate the quantitative relationships between operational factors—contact time (A), pH (B), and initial concentration (C)—and the various water quality responses. For TDS and EC, the models predict values ranging from approximately 198 to 841 mg·L^{-1} and 430 to 1701 µS·cm^{-1}, respectively, indicating strong sensitivity to pH and concentration, with notable quadratic effects evident in B^2 and C^2 terms. These trends are consistent with findings by Abushandi, (2025), who reported nonlinear increases in dissolved solids with higher pH and pollutant loadings. Dissolved oxygen exhibited predicted ranges of 11.0–11.8 mg·L^{-1}, with minor quadratic effects, reflecting the modest but significant role of time and concentration in oxygen retention. BOD and COD values ranged from 8.4–14 mg·L^{-1} and 160–235 mg·L^{-1}, respectively, with BOD showing minor curvature while COD displayed stronger quadratic dependence on concentration. Similarly, Zn and Mn predictions varied from 1.15–1.95 mg·L^{-1} and 0.055–0.125 mg·L^{-1}, demonstrating clear interactions between pH and time, consistent with metal adsorption dynamics. The mineral parameters, including alkalinity, hardness, and calcium, ranged from 120–162 mg·L^{-1}, 62–95 mg·L^{-1}, and 1.45–2.2 mg·L^{-1}, showing linear increases with time and pH, while total solids varied between 4–10.9 g·L^{-1}, highlighting the combined influence of all operational factors on effluent characteristics. These predictive models provide a robust framework for optimizing treatment performance under varying operational conditions.

$$TDS = 388.20190 - 0.152656A - 27.83504B - 0.320098C - 1.85 \times 10^{-6}AB + 7.40 \times 10^{-8}AC + 2.22 \times 10^{-6}BC + 0.000288A^2 + 1.59523B^2 + 0.000859C^2 \quad (1)$$

$$EC = 806.43792 - 0.289504A - 58.50890B - 0.563406C + 1.65 \times 10^{-15}AB - 1.48 \times 10^{-7}AC + 1.25 \times 10^{-15}BC + 0.000646A^2 + 3.39678B^2 + 0.001726C^2 \quad (2)$$

$$DO = 8.73400 + 0.002658A + 0.662632B + 0.000027C - 9.50 \times 10^{-6}A^2 - 0.042576B^2 - 0.000018C^2 \quad (3)$$

$$BOD = 19.45966 - 0.021550A - 1.86102B + 0.009895C + 0.002965AB - 0.000104AC - 0.001482BC + 0.000044A^2 + 0.112042B^2 + 0.000091C^2E \quad (4)$$

$$COD = 330.85640 - 0.002914A - 34.25316B - 0.197832C + 0.009257AB - 0.000864AC + 0.011113BC + 0.000134A^2 + 2.08476B^2 + 0.002581C^2B \quad (5)$$

$$Zn = 4.37186 + 0.002597A - 0.920328B + 0.009161C - 0.000535AB - 0.000074AC - 0.001864BC + 0.000057A^2 + 0.068737B^2 + 0.000089C^2 \quad (6)$$

$$Mn = 0.393179 + 0.000190A - 0.093811B + 0.000716C - 0.000044AB - 6.67 \times 10^{-6}AC - 0.000173BC + 5.38 \times 10^{-6}A^2 + 0.006888B^2 + 9.26 \times 10^{-6}C^2 \quad (7)$$

$$Alkalinity = 53.09081 + 0.507513A + 8.87436B + 1.02047C - 0.022841AB - 0.003753AC - 0.093333BC \quad (8)$$

$$Hardness = 10.42708 + 0.395145A + 6.88337B + 0.803487C - 0.017593AB - 0.003025AC - 0.072964BC \quad (9)$$

$$Ca = 0.283019 + 0.008779A + 0.159351B + 0.018259C - 0.000394AB - 0.000066AC - 0.001678BC \quad (10)$$

$$TS = 10.91243 - 0.019451A - 1.47828B + 0.006918C + 0.002067AB - 0.000073AC - 0.001000BC + 0.000078A^2 + 0.083398B^2 + 0.000054C^2 \quad (11)$$

3.4.3 Response surface plots

The response surface patterns generated reveal clear differences in how each variable responded to changes in pH, initial concentration, and contact time. For TDS and EC, the surfaces showed pronounced curvature driven largely by pH^2, consistent with the significant model outcomes ($p = 0.0008$ and 0.0015) as illustrated in (a) and (b) respectively. The plots illustrated steep gradients at lower pH levels and shorter contact times, confirming that all three linear factors shaped their behaviour. Furthermore, the DO response surface demonstrated smooth but notable shifts across the factor space, particularly along the contact time and concentration axes as shown in (c). The surface curvature reinforced the statistical significance of pH^2, suggesting that oxygen depletion or retention was strongly tied to the interactive chemistry of the system.

The surfaces generated for BOD and COD highlighted distinct behavioural tendencies as illustrated in (d) and (e) respectively. The BOD plot displayed minimal variation across the response plane, aligning with its statistically non-significant model ($p = 0.1875$). Only mild curvature associated with pH^2 was visible, indicating limited responsiveness across the studied factor ranges. In contrast, the COD surface manifested more defined gradients, especially with increasing concentration, confirming the dominant role of concentration and its quadratic contribution as depicted in (f). Likewise, the Zn and Mn response surfaces revealed strong curvature across all axes, reflecting their significant models and the influence of A^2, B^2, and C^2. Time emerged as a key factor, with the surfaces showing higher removal efficiency at extended contact durations, consistent with metal uptake mechanisms commonly reported in adsorption studies as shown in (f) and (g).

The surfaces for alkalinity, hardness, and calcium presented more complex but less intense variations. Although their models were not statistically significant, the response plots exhibited visible interaction effects between pH and concentration, matching the AC interaction highlighted in the analysis. The contours were neither flat nor sharply sloped, indicating that these parameters reacted to combined operational changes rather than individual factors acting alone. This interaction-driven behaviour aligns with earlier observations by Singh, (2024), who reported that mineral ions often show secondary responsiveness influenced more by synergistic effects. Finally, the response surface for total solids (TS) displayed pronounced curvature and distinct ridges shaped by time, A^2 and B^2, and the AB and AC interactions. The shape of the surface confirmed a highly interdependent system where solids removal varied dynamically across the operational domain, consistent with the complexity typical of heterogeneous industrial effluents.

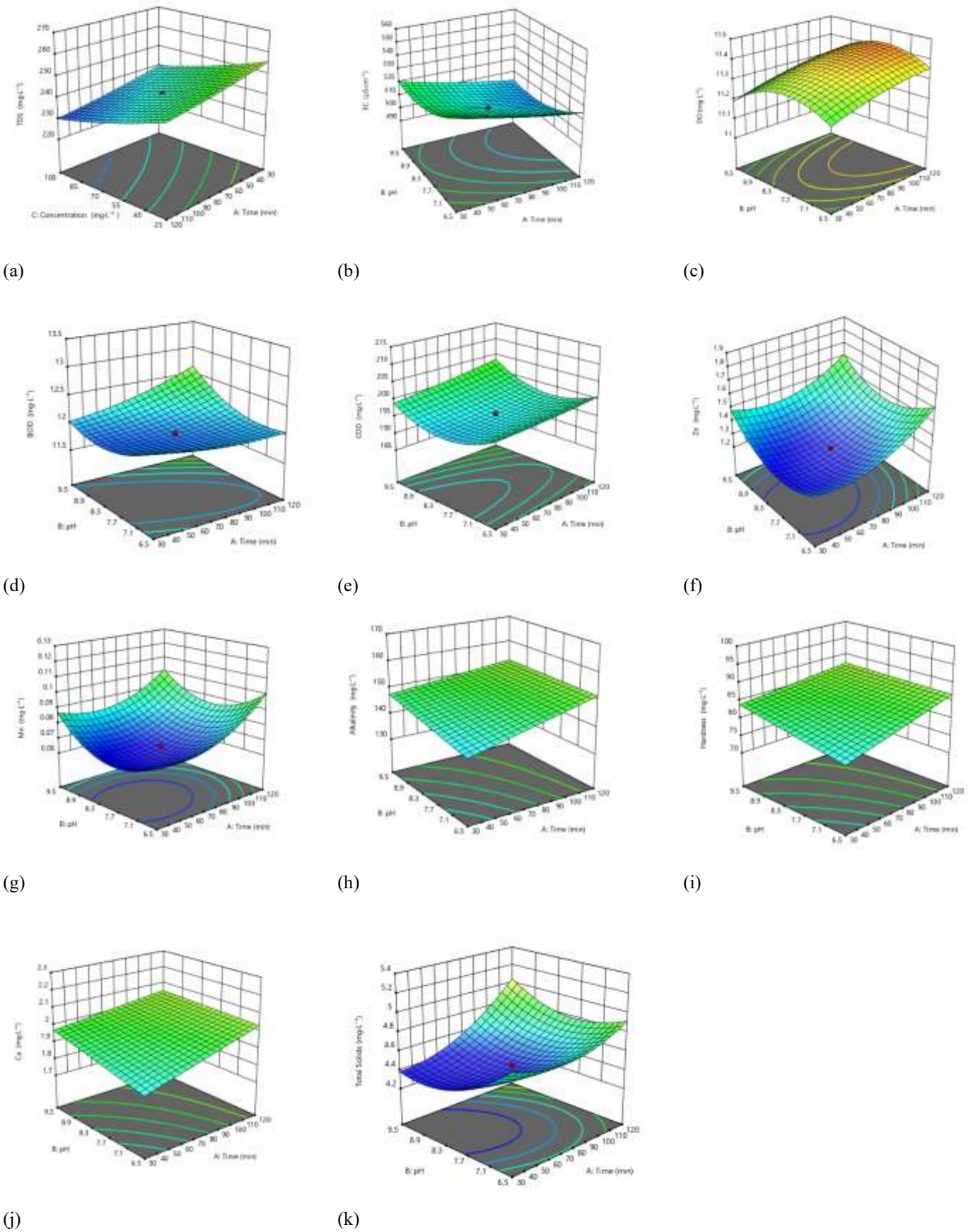

Figure 2: Response surface plots for all measured water-quality parameters, showing: (a) TDS, (b) EC, (c) DO, (d) BOD, (e) COD, (f) Zn, (g) Mn, (h)Alkalinity, (i) Hardness, (j) Calcium, and (k) Total Solids.

4. CONCLUSION

The silver nanoparticles (AgNPs) synthesized in this study exhibited uniform morphology with particle sizes ranging from 15 to 25 nm, confirming their suitability for heavy metal adsorption. Characterization of heavy metals in the marble effluent revealed that Zn and Pd concentrations were effectively reduced from 4.3–5.0 mg/L and 0.08–0.12 mg/L to 1.8–1.9 mg/L and 0.03–0.05 mg/L, respectively, whereas Mn and Cd increased from 0.18–0.18 mg/L and 0.002–0.003 mg/L to 0.65–0.65 mg/L and 0.012–0.14 mg/L, indicating selective removal. Process optimization showed that TDS (320–324 mg/L to 835–841 mg/L), EC (651–656 µS/cm to 1680–1701 µS/cm), and DO (12–13 mg/L to 9–10.5 mg/L) were significantly influenced by contact time, pH, and initial concentration. Regression models accurately predicted responses, highlighting the strong quadratic effect of pH (6.5–9.5) and concentration (25–100 mg/L) on several parameters. Response surface plots further confirmed that optimal removal efficiencies for Zn and Pd were achieved within these ranges. Overall, AgNPs demonstrated high potential for heavy metal remediation under controlled conditions.

REFERENCES

1. Abushandi, E. (2025). Water Quality Assessment and Forecasting Along the Liffey and Andarax Rivers by Artificial Neural Network Techniques Toward Sustainable Water Resources Management. Water, 17(3), 453.
2. Ali, A., Mannan, A., Hussain, I., Hussain, I., and Zia, M. (2018). Effective removal of metal ions from aquous solution by silver and zinc nanoparticles functionalized cellulose: Isotherm, kinetics and statistical supposition of process. Environmental Nanotechnology, Monitoring and Management, 9, 1-11.
3. Ambaye, T. G., Vaccari, M., van Hullebusch, E. D., Amrane, A., and Rtimi, S. J. I. J. O. E. S. (2021). Mechanisms and adsorption capacities of biochar for the removal of organic and inorganic pollutants from industrial wastewater. International Journal of Environmental Science and Technology, 18(10), 3273-3294.
4. Arslan, E. I., Aslan, S., Ipek, U., Altun, S., and Yazicioğlu, S. (2005). Physico-chemical treatment of marble processing wastewater and the recycling of its sludge. Waste management and research, 23(6), 550-559.
5. Asemave, K., Thaddeus, L., and Tarhemba, P. T. (2021). Lignocellulosic-based sorbents: a review. Sustainable Chemistry, 2(2), 271-285.
6. Asimullah, S., Afridi, J., and Hayat, S. (2025). Environmental Impacts of Marble Industrial Effluents on Water and Soil in Tehsil Shabqadar, Khyber Pakhtunkhwa. Indus Journal of Bioscience Research, 3(3), 370-376.
7. Boyle, O., Xiao, B., and Mangwandi, C. (2025). Valorization of banana peel waste into advanced adsorbent beads for the removal of emerging pollutants from wastewater. Materials, 18(5), 1084.
8. Brears, R. C. (2025). Sustainable Water-Food Nexus: Circular Economy, Water Management, Sustainable Agriculture. Walter de Gruyter GmbH and Co KG.
9. Covington, M. D., Martin, J. B., Toran, L. E., Macalady, J. L., Sekhon, N., Sullivan, P. L., and Graham, W. D. (2023). Carbonates in the critical zone. Earth's Future, 11(1), e2022EF002765.
10. Ejairu, U., Aderamo, A. T., Olisakwe, H. C., Esiri, A. E., Adanma, U. M., and Solomon, N. O. (2024). Eco-friendly wastewater treatment technologies (concept): Conceptualizing advanced, sustainable wastewater treatment designs for industrial and municipal applications. Comprehensive research and reviews in Engineering and Technology, 2(1), 083-104.
11. Esmaeeli, A., Sarrafzadeh, M. H., Zeighami, S., Kalantar, M., Bariki, S. G., Fallahi, A., and Ghaffari, S. B. (2023). A comprehensive review on pulp and paper industries wastewater treatment advances. Industrial and Engineering Chemistry Research, 62(21), 8119-8145.
12. Gupta, S. S., Al Kausor, M., and Chakrabortty, D. (2025). Banana peel as potential bioadsorbent toward removal of emerging contaminants from wastewater for sustainable environment: a review. Chemical Papers, 1-34.
13. Hou, L., Liang, Q., and Wang, F. (2020). Mechanisms that control the adsorption–desorption behavior of phosphate on magnetite nanoparticles: the role of particle size and surface chemistry characteristics. RSC advances, 10(4), 2378-2388.
14. Ismail, W. W., Syah, M. I. A. I., Muhet, N. H. A., Bakar, N. A., Yusop, H. M., and Samah, N. A. (2022). Adsorption behavior of heavy metal ions by hybrid inulin-TEOS for water treatment. Civil Engineering Journal, 8(9), 1787-1798.
15. Khan, N. H., Nafees, M., Saeed, T., Zuljajal, F., Akbar, H., and Rehman, A. (2023). Marble Production and Environmental Pressure: A Case Study of Hayatabad Industrial Estate Peshawar, Pakistan.
16. Kunwar, P. (2022). Commercialization challenges of adsorbent materials for water and wastewater treatment (Master's thesis, P. Kunwar).

17. Lin, L., Jiang, W., Xu, X., and Xu, P. (2020). A critical review of the application of electromagnetic fields for scaling control in water systems: mechanisms, characterization, and operation. NPJ Clean Water, 3(1), 25.
18. Mansour, A. T., Alprol, A. E., Abualnaja, K. M., El-Beltagi, H. S., Ramadan, K. M., and Ashour, M. (2022). The using of nanoparticles of microalgae in remediation of toxic dye from industrial wastewater: kinetic and isotherm studies. Materials, 15(11), 3922.
19. Noreen, U., Ahmed, Z., Khalid, A., Di Serafino, A., Habiba, U., Ali, F., and Hussain, M. (2019). Water pollution and occupational health hazards caused by the marble industries in district Mardan, Pakistan. Environmental Technology and Innovation, 16, 100470.
20. Obiuto, N. C., Olu-lawal, K. A., Ani, E. C., Ugwuanyi, E. D., and Ninduwezuor-Ehiobu, N. (2024). Chemical engineering and the circular water economy: Simulations for sustainable water management in environmental systems. World journal of advanced research and reviews, 21(3), 001-009.
21. Ruan, T., Li, P., Wang, H., Li, T., and Jiang, G. (2023). Identification and prioritization of environmental organic pollutants: From an analytical and toxicological perspective. Chemical Reviews, 123(17), 10584-10640.
22. Sathasivam, J., Kumar, A., and Narayanasamy, S. (2024). Valorisation of Agricultural Waste into a Low-Cost Adsorbent: Perspective of Reutilization. In Agricultural Waste to Value-Added Products (pp. 125-149). Springer, Singapore.
23. Sathya, K., Nagarajan, K., Carlin Geor Malar, G., Rajalakshmi, S., and Raja Lakshmi, P. (2022). A comprehensive review on comparison among effluent treatment methods and modern methods of treatment of industrial wastewater effluent from different sources. Applied Water Science, 12(4), 70.
24. Sati, A., Ranade, T. N., Mali, S. N., Ahmad Yasin, H. K., and Pratap, A. (2025). Silver nanoparticles (AgNPs): comprehensive insights into bio/synthesis, key influencing factors, multifaceted applications, and toxicity─ a 2024 update. ACS omega, 10(8), 7549-7582.
25. Singh, A. K. (2024). Impacts of Minerals on the Plant's Growth and Metabolism. Addition Publishing House.
26. Syafiuddin, A., Fulazzaky, M. A., Salmiati, S., Kueh, A. B. H., Fulazzaky, M., and Salim, M. R. (2020). Silver nanoparticles adsorption by the synthetic and natural adsorbent materials: an exclusive review. Nanotechnology for Environmental Engineering, 5(1), 1.
27. Thakur, A., and Kumar, A. (2024). Innovative technologies for the removal of pollutants in the chemical industries. In Innovative and hybrid technologies for wastewater treatment and recycling (pp. 167-195). CRC Press.
28. van Linden, N., Bandinu, G. L., Vermaas, D. A., Spanjers, H., and van Lier, J. B. (2020). Bipolar membrane electrodialysis for energetically competitive ammonium removal and dissolved ammonia production. Journal of Cleaner Production, 259, 120788.